Journal of Chromatography A 1749 (2025) 465877

Contents lists available at ScienceDirect

Journal of Chromatography A

journal homepage: www.elsevier.com/locate/chroma

Advancing profiling of secondary antioxidant metabolites in *Allium cepa* PDO leaf extract: Online comprehensive two-dimensional liquid chromatography with high-resolution mass spectrometry and pre-column DPPH assay

Giovanna Aquino [a,b], Eduardo Maria Sommella [a], Emanuela Salviati [a,*], Michele Manfra [c], Giulia Auriemma [a], Pietro Campiglia [a], Giacomo Pepe [a], Manuela Giovanna Basilicata [d]

[a] Department of Pharmacy, University of Salerno, Via Giovanni Paolo II, Fisciano, 84084 Salerno, Italy
[b] PhD Program in Drug Discovery and Development, University of Salerno, Fisciano, 84084 Salerno, Italy
[c] Department of Health Sciences, University of Basilicata, Viale dell'Ateneo Lucano 10, 85100 Potenza, Italy
[d] Department of Advanced Medical and Surgical Sciences, University of Campania "Luigi Vanvitelli", Naples, Italy

ARTICLE INFO

Keywords:
Agri-food waste, LC×LC-HRMS
Peak capacity
Orthogonality
DPPH-LC×LC offline

ABSTRACT

The food and agricultural processing industries generate significant amounts of phenolic-rich by-products, which hold potential as natural antioxidant sources for a wide range of applications, including functional ingredients and nutraceutical formulations. *Allium cepa* leaves represent a promising source of bioactive compounds. However, due to the complexity of their chemical composition, advanced analytical techniques are required to fully characterize the secondary metabolite profile and identify specific phytochemical classes or fractions with high nutraceutical potential. In this context, an online comprehensive two-dimensional liquid chromatography (LC×LC) approach was developed and optimized for the in-depth characterization of the phytochemical profile of *Allium cepa* PDO leaf extract. Key parameters in both dimensions, including flow rate, stationary phase chemistry, and mobile phase composition, were investigated to enhance peak capacity and orthogonality. The optimized method combined reversed phase in both dimension (RP-LC×RP-LC), offering high orthogonality (A_O: 70.46 %) and peak capacity (n_c: 1788.88). and significantly improving the separation of multiple secondary metabolite classes by effective employment of the 2D separation space. Further hyphenation with high-resolution mass spectrometry (HRMS), enhanced compound annotation compared to mono-dimensional (1D-LC) techniques. A total of 147 compounds were tentatively annotated belonging to multiple classes such as flavonoids, saponins, phenylpropanoids, isoprenoids, terpenes, dipeptides, fatty acids, and lipids. Additionally, the antioxidant activity of *Allium cepa* leaf extract was assessed by coupling a pre-column 2,2-diphenyl-1-picrylhydrazyl (DPPH) assay with the LC×LC-DAD-HRMS platform. This integrated approach enabled the identification of individual contributions of flavonoids, isoprenoids, and phenylpropanoids to radical scavenging activity.

The method allowed an in-depth exploration of *Allium cepa* phytochemical profile, demonstrating to hold significant potential for the standardization of antioxidant biomarkers, with promising applications in the nutraceutical industry.

1. Introduction

Agri-food waste (AFW), such as peels, seeds, and leaves, are among the most common by-products generated during fruit and vegetable processing. Traditional applications for these wastes include their use as soil fertilizers, animal feed, or biomass for producing energy and fuels [1]. However, AFW is extremely rich in various bioactive components, such as phenolic acids, flavonoids, and saponins, which are of significant interest for human health due to their antioxidant and anti-inflammatory properties, particularly in preventing metabolic

* Corresponding author.
E-mail addresses: gaquino@unisa.it (G. Aquino), esommella@unisa.it (E.M. Sommella), esalviati@unisa.it (E. Salviati), michele.manfra@unibas.it (M. Manfra), gauriemma@unisa.it (G. Auriemma), pcampiglia@unisa.it (P. Campiglia), gipepe@unisa.it (G. Pepe), manuelagiovanna.basilicata@unicampania.it (M.G. Basilicata).

https://doi.org/10.1016/j.chroma.2025.465877
Received 30 January 2025; Received in revised form 12 March 2025; Accepted 13 March 2025
Available online 14 March 2025

diseases [2].

Recovering these high-value-added components from the matrix requires effective extraction methods. Both conventional and advanced techniques, such as solid-liquid extraction, pressurized liquid extraction, and green approaches like microwave and supercritical fluid extraction, can be employed [3]. Beyond extraction, the chemical characterization of AFW is crucial. To standardize recovery processes and facilitate their further valorization and transformation into high-value nutraceutical or cosmeceutical products, it is essential to thoroughly define their chemical profile [4]. This task is challenging because these samples often contain a wide array of chemically diverse compounds, making accurate characterization difficult. This is particularly true for less abundant secondary metabolites, which hold significant potential for human health applications.

Liquid chromatography (LC) is the most widely used method for analyzing food and food by-products. When coupled with the power of mass spectrometry (MS), it serves as the gold standard for profiling secondary metabolites in food matrices [5]. However, conventional one-dimensional LC methods (1D-LC) often fail to resolve the chemical complexity of these matrices, which results in issues such as MS overload due to multiple co-elutions and ion-suppression phenomena, which obscure the detection of minor components [6]. Two-dimensional LC approaches (2D-LC), particularly in the comprehensive mode (LC×LC), have emerged as innovative methods for food analysis [7]. LC×LC approaches have been successfully applied to characterizing food waste using various stationary phase combinations. For example, reversed phase × reversed phase (RP×RP) has been employed for analyzing pyrolysis-derived bio-oils and dairy waste [8,9], while hydrophilic interaction chromatography × reversed phase (HILIC×RP) has been applied to grape seeds, grapevine canes, and black chokeberry pomaces [10–12]. In the context of AFW valorization, we recently investigated the secondary metabolite profile of *Allium cepa* leaves using a Box–Behnken design-guided microwave-assisted extraction (MAE) combined with LC—HRMS [13]. Given the complex, multi-component nature of *A. cepa* leaves, achieving higher chromatographic resolution is critical. An LC×LC approach could address this challenge, requiring careful optimization of method parameters to fully utilize the 2D separation space [14]. In this study, we aim to enhance the chemical characterization of this food waste by developing and optimizing an RP×RP method coupled with HRMS. This approach will demonstrate significant advantages over conventional 1D-LC methods. Furthermore, integrating a pre-column DPPH assay with LC×LC will provide deeper insights into the antioxidant components of the hydroalcoholic extract.

2. Materials and methods

2.1. Reagents and materials

Solvents and additives: Water suitable for LC/MS, LiChrosolv®, acetonitrile (ACN) hypergrade for LC-MS LiChrosolv®, acetic acid and formic acid for LC-MS LiChropur™, 2,2-Diphenyl-1-picrylhydrazyl, ferulic acid were purchased from Merck (Milan, Italy).

Standards: Quercetin-3,4′-di-*O*-glucoside and kaempferol-3-*O*-glucoside were purchased from Extrasynthese (Z.I Lyon Nord, France). Azelaic acid and phloridzin dihydrate were purchased from Kema Science (Naples, Italy).

Columns: Kinetex Biphenyl, 100 Å (100×2.1 mm×1.7 μm), Kinetex EVO C18, 100 Å (100×2.1 mm×2.6 μm), Kinetex C18, 100 Å (100×2.1 mm×2.6 μm), Core-Shell from Phenomenex, Torrance, CA, USA. InfinityLab Poroshell 120 Bonus-RP, 120 Å (50×3.0 mm×2.7 μm), InfinityLab Poroshell 120 HILIC, 120 Å (100×2.1 mm×2.7 μm), Superficially Porous; ZORBAX RRHD Eclipse Plus C18, 95 Å (50×3.0 mm×1.8 μm), Fully Porous from Agilent Technologies, Santa Clara, CA, USA. Titan™, 80 Å (50×3.0 mm×1.9 μm), Totally Porous from Supelco, Bellefonte, PA, USA. Acquity UPLC® BEH Amide, 130 Å (100×2.1 mm×1.7 μm) from Waters Corporation, Milford, MA, USA.

2.2. Sample preparation

Allium cepa leaves were kindly donated by consortium for the protection of "*Cipollotto* (spring onions) *Nocerino* DOP".

Allium cepa PDO (Protected Designation of Origin) leaves hydroalcoholic extract was obtained using a previously optimized Box Behnken Design – Microwave Assisted Extraction model (**Supplementary Materials**) [13]. For the two-dimensional LC analyses, 140 mg of extract were dissolved in 1 mL of methanol/water mixture (50:50 v/v) and then centrifuged at 5000 g for 5 min. The supernatant was collected and injected into the LC system.

2.3. LC × LC instrumentation

A comprehensive two-dimensional liquid chromatography instrumentation was assembled for the ^{1}D separation using a 1260 Infinity autosampler module (G7129A), a 1260 Infinity capillary pump (G7112B), a column compartment (G7116A), and a VWD detector module (G7114B). The ^{2}D was constituted by a 1290 Infinity II high speed pump (G7120A) and a DAD detector (G7117B). Both dimensions were connected by a valve drive (G1170A) equipped with 5-position/10-port 2D-LC active solvent modulation (ASM) valve coupled to two 6-position/14-port valve heads equipped with six 40 μL loops each (#5067–5926 Capillary 0.35 × 420 mm). The ASM valve contained the ASM capillary of dimension 0.12 × 170 mm (1.9 μL, #5500–1301) (ASM factor 3). The 2D-LC system was controlled by Agilent OpenLab CDS ChemStation Rev. LTS.01.11. Separations were recorded at 280 and 330 nm although, in addition, UV–Vis spectra were collected from 190 to 400 nm at a sampling rate of 80 Hz in the DAD.

2.4. LC×LC separation conditions

In preliminary experiments, different ^{1}D and ^{2}D stationary phases were evaluated (see afterwards). The final RP×RP setup comprised:

^{1}D separation: a Kinetex 1.7 μm Biphenyl 100 Å, LC Column 100 × 2.1 mm (Phenomenex, Torrance, CA, USA) column. Acidified water (0.1 % acetic acid, *v/v*, A) and methanol (0.1 % acetic acid, *v/v*, B) were used as mobile phases. Under optimum conditions, the gradient was: 0.00 min, 2 % B; 15 min, 30 % B; 40 min, 40 % B; 100 min, 65 % B; 120 min, 90 % B; 125 min, 90 % B, then 30 min of post-time. The flow rate was set at 50 μL min^{-1}, the column temperature at 40 °C and the injection volume was 2 μL.

^{2}D separation: An Agilent InfinityLab Poroshell 120 Bonus-RP 2.7 μm, LC Column 3.0 × 50 mm was employed. Acidified H_2O (0.1 % acetic acid, solvent A) and ACN (0.1 % acetic acid, solvent B) were selectedas mobile phases. The flow rate and the column temperature were set at 2.5 mL min^{-1} and 50 °C respectively.

2D Gradient was operated in segmented shifting mode (see Section 3.3 afterwards).

2.5. Peak capacity calculations

The performance of the different combinations was compared in terms of peak capacity values (n_c) and orthogonality. The ^{1}D peak capacity in gradient conditions was calculated according to Eq. (1):

$$1n_c = \frac{(1t_{r,f} - 1t_{r,i})}{1w_{avg}} \quad (1)$$

where $t_{r,f}$ and $t_{r,i}$ are the retention times of the final and initial peaks eluting in the ^{2}D map, and w_{avg} is the average 4σ peak width of five selected peaks in the ^{2}D map, covering the whole separation window in the ^{2}D space.

The ^{2}D peak capacity was calculated according to Eq. (2):

$$2n_c = \frac{2t_g}{2w_{avg}} \quad (2)$$

where $2t_g$ represents the second-dimension gradient time, excluding the re-equilibration time, and w_{avg} is the average 4σ peak width of the second-dimension separation, determined using the same peaks employed for the ^1n_c calculation. The theoretical peak capacity of the two-dimensional system can be calculated by multiplying the individual peak capacities obtained for the two dimensions, following the so-called "product rule" [15], according to Eq. (3):

$$2Dn_c = 1n_c \times 2n_c \quad (3)$$

Eq. (3) is well known to significantly overestimate the practical peak capacity of the system [15–18]. To achieve more accurate results, it is essential to account for the undersampling effect. This correction is implemented by applying the Davis-Stoll-Carr factor [16,19] to the "product rule" (Eq. (3)), as outlined in Eq. (4) and 5:

$$\langle\beta\rangle = \sqrt{1 + 3.35\left(\frac{2t_c 1n_c}{1t_g}\right)^2} \quad (4)$$

$$2Dn'_c = \frac{(1n_c \times 2n_c)}{\langle\beta\rangle} \quad (5)$$

where $\langle\beta\rangle$ is the undersampling correction factor, $2t_c$ is second dimension cycle time (which is equal to the second-dimension gradient time, plus the second-dimension re-equilibration time), $1t_g$ is the first-dimension gradient time and $2Dn'_c$ is the effective peak capacity.

Over the years, various methods have been developed to quantify orthogonality, primarily as metrics for optimizing and comparing comprehensive 2D separations. Among these, the bin method proposed by Gilar [20], as well as the convex-hull [21] together with the fractional coverage [22] are all valid approaches to estimate the solute occupation of the 2D space. However, these methods require programming skills and algorithmic implementation, making them less accessible for simple Excel-based calculations.

Therefore, we chose the asterisk equations method to estimate orthogonality (A_0), providing a measure of the method's performance [23]. This value was then used to correct the effective peak capacity ($2Dn'_c$) values, as shown in Eq. (6):

$$2Dn_{c,corrected} = 2Dn'_c \times A_0 \quad (6)$$

2.6. Precision assessment of 2D-LC method

The precision of the optimized 2D-LC method was evaluated through intraday and interday experiments. Five representative standards were selected for the repeatability assessment: quercetin-3,4′-di-*O*-glucoside (1), ferulic acid (2), phloridzin dihydrate (3), kaempferol-3-*O*-glucoside (4), and azelaic acid (5). Additionally, five representative peaks from the *Allium cepa* leaf extract (blobs 1, 8, 10, 11, and 16) were chosen across the separation space.

Intraday repeatability was assessed by analyzing the extract and standards using 2D-LC at three different time points within the same day. Intermediate precision was evaluated under the same experimental conditions after six days. Precision for both dimensions of separation was determined by calculating the coefficient of variation (CV) for the retention times and peak areas of the five selected peaks from both the sample and standards across the 2D separation space.

2.7. LC× LC-ESI-HRMS-MS/MS conditions

The RP-LC × RP-LC system was coupled online to a hybrid quadrupole Orbitrap Exploris ™ 120 mass spectrometer (Thermo Fisher Scientific, Bremen, Germany) equipped with a heated electrospray ionization probe (HESI II) operating in negative and positive ionization mode.

The MS was calibrated by Thermo Pierce™ FlexMix™ Calibration Solutions in both polarities. Full MS (100–1500 m/z) and data-dependent MS/MS were performed at a resolution of 30,000 and 15,000 FWHM respectively; Normalized HCD Collision Energies (%) of 20, 40 and 60 were used. Source parameters: Sheath gas pressure, 50 arbitrary units; auxiliary gas flow, 15 arbitrary units; spray voltage, +3.4 kV, −3.3 kV; capillary temperature, 300 °C; auxiliary gas heater temperature, 340 °C.

2.8. LC× LC-DAD-HRMS-MS/MS data analysis

LC image™ software v2024r1 LC×LC (GC Image®, LLC, Lincoln NE, USA) was used to plot the results as 2D and 3D images.

Peaks annotations were carried out by comparing their MS/MS fragmentation pattern with libraries as well as with reported data in literature, and, when available with retention times of external standards. The identification level was established according to Metabolomics Standards Initiative (MSI): level 1, unambiguous identification with reference standards; level 2, putative identification by matching MS2 data to literature data or spectral databases; level 3, putative identification established by spectral similarity to chemical class of compounds and chemotaxonomic [24].

For HRMS data analysis and processing, FreeStyle™ 1.8 SP2 and Compound Discoverer™ 3.1 software (Thermo Scientific, SanJose, CA, U.S.A.) were used for raw data processing (baseline correction, noise filtering, spectral alignment, and peak detection) and for putative identification of metabolites based on molecular formula (matched), exact mass (mass tolerance <5 ppm) and MS2 fragmentation pattern [Fragment Ion Search (FISh)], with a global database search (mzCloud, MassList and ChemSpider). Other databases, containing fragmentation spectrum information of natural product molecules from different sources, mainly include MassBank (https://massbank.eu/MassBank/), GNPS (https://gnps.ucsd.edu/ProteoSAFe/static/gnps-splash.jsp/), PubChem (https://pubchem.ncbi.nlm.nih.gov/), LipidMAPS (http://www.lipidmaps.org/), FooDB (http://foodb.ca/), Phenol-Explorer (http://phenol-explorer.eu/), PlantaeDB (https://plantaedb.com/), PMhub (https://pmhub.org.cn/#/) and LOTUS (https://lotus.naturalproducts.net/).

To obtain more information about the chemical profile of the investigated extract, further processing was carried out using MZmine (version 4.4.3) [25]. An untargeted LC-MS/MS workflow was applied by performing a processing mzwizard by selected UHPLC system and MS Orbitrap type. After the final aligned feature list, spectral library search was performed to annotate compounds by matching features with spectral libraries such as MoNA (https://mona.fiehnlab.ucdavis.edu/), GNPS (https://gnps.ucsd.edu/ProteoSAFe/static/gnps-splash.jsp/) and the freely available MSnLib Mass spectral libraries (.mgf) on Zenodo (https://zenodo.org/records/11163381) [26].

All parameters for Compound Discoverer and MZmine workflows are summarized in **Tables S1** and **S2**, respectively.

2.9. Precolumn DPPH-LC× LC- radical scavenger activity evaluation

The determination of antioxidant capacity of *Allium cepa* leaf extract was carried out as reported previously, with slight modifications [27]. Two hundred microliters of sample were added to 2,2-diphenyl-1-picrylhydrazyl (DPPH) solution (5 mM) in a 1:1 (*v*/*v*) ratio. The mixture was briefly sonicated then left to react for 30 min (t) in the dark at room temperature. The sample was filtered through 0.45 μm and injected in the RP-LC × RP-LC optimized system under the same conditions reported above. To avoid sample dilution caused by mixing with DPPH and to accurately monitor the decrease in UV peak intensity due to radical quenching, 200 μL of the extract was diluted in a 1:1(*v*/*v*) ratio with methanol and used as control (0).

Under these conditions, the chromatographic peak areas were

monitored at 280 nm and 330 nm and integrated to calculate the radical scavenging activity (RSA) with the following Eq. (7):

$$RSA(\%) = \frac{PA_{(0)} - PA_{(t)}}{PA_{(0)}} \times 100 \quad (7)$$

where $PA_{(0)}$ is referred to the chromatographic peak area of the extract solution diluted with methanol (control), whereas $PA_{(t)}$ is referred to the peak area of extract solution after mixed incubation with the DPPH solution.

3. Results

3.1. Stationary phase selection and LC parameters optimization for the ^1D

Choosing the right chromatographic column combination is a critical factor in LC×LC. The performance of the columns in the first and second dimensions significantly influences the overall peak capacity and the correlation of peak distribution [28]. Based on prior knowledge of the compound classes present in the extract, obtained through previous 1D-LC characterizations [13], a reversed-phase (RP) approach was chosen over HILIC in the ^{1}D separation. This choice was driven by the limited utility of a HILIC phase for the specific sample under investigation, as can be observed from the unsatisfactory separation of the whole extract that showed poor retention on two different stationary phases, namely bare silica and amide (**Figure S1**). Although HILIC × RP coupling is well-established for delivering high levels of orthogonality in comprehensive 2D chromatographic separations [29], the expected chemical classes in the extract drove the choice toward an RP × RP platform. In LC × LC, usually a low-flow ^{1}D separation is combined with a long and shallow gradient as often the starting point. This approach allows for adequate sampling of ^{1}D peaks while ensuring the transfer of small volumes on to of ^{2}D column, enhancing peak focusing.

The choice of ^{1}D RP stationary phase focused on the use of two core-shell columns with different stationary phase chemistries. Specifically, a core shell EVO C18 column was compared against a core shell Biphenyl column. Initially two different flow rates were tested 100 and 50 µL/min starting with long gradients of 280 and 140 min. Previous studies emphasized the differing separation mechanisms C18 and Biphenyl stationary phases, with the Biphenyl phase offering distinct selectivity for compounds with aromatic structures through π-π interactions. Additionally, compared to ACN, MeOH enhances π-π interactions, as previously demonstrated [30]. Indeed, the Biphenyl column, with methanol as organic modifier delivered superior performance compared to the EVO C18 column (Fig. 1), and generally higher retention for compounds eluting after 35 min as well adifferent selectivity and resolution for compounds eluting in the last retention time window comprised between 75-to 100 min, maximizing the efficient use of the one-dimensional chromatographic space. Furthermore, to achieve a more accurate determination of peak capacity for the two mono-dimensional systems, we performed calculations using a mixture of standards (**Figure S2**). The comparison of peak capacities yielded an n_c value of 165 for EVO C18, while 218 for Biphenyl, hence the Biphenyl column was finally selected for ^{1}D. Since loop configuration was kept fixed at 40 µL, in order to fill at least 80 % of the loop, a modulation time of 0.64 min was selected, and thus the ^{1}D was finally operated at 50 µL/min.

3.2. Stationary phase selection and LC parameters optimization for the ^2D

Since the same separation mode (RP) was used, a key aspect for RP × RP separations is maximizing the orthogonality. For this purpose, different ^{2}D columns were evaluated, characterized by specific chemical and physical differences such as, packed with both core-shell and fully porous particles, and with traditional embedded C-18 phase as well as modified polar reversed-phase with an embedded amide linkage. In contrast, column geometry was kept fixed (L. × *I*.D., 50 × 3.0 mm). Detailed characteristics are summarized in Section 2.1.

Additionally, two different organic modifiers (MeOH and ACN) and acidic additive conditions (HCOOH and CH_3COOH, 0.1 %) were evaluated, as well as three different flow rates (2, 2.2, 2.5mL/min), to achieve a fast ^{2}D cycle, were also tested.

As shown in Fig. 2, among the investigated conditions the

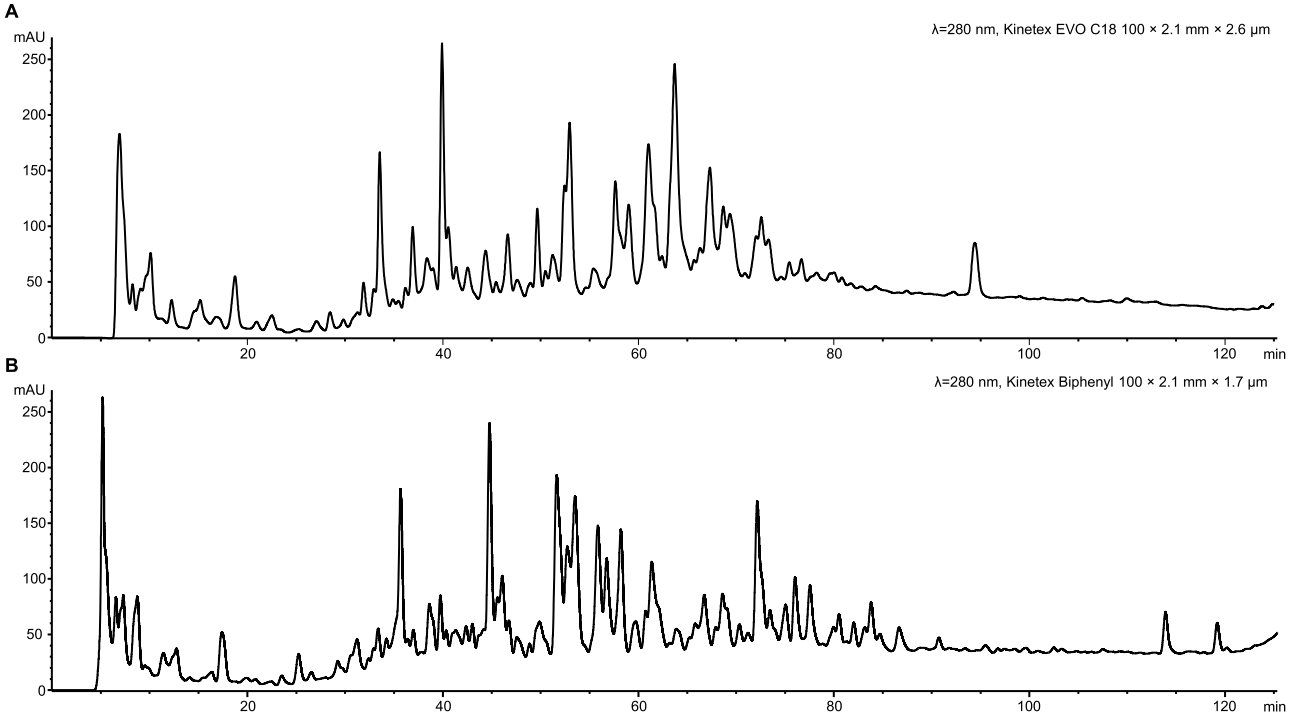

Fig. 1. ^{1}D-RP-VWD separation (λ=280 nm) achieved by Kinetex EVO C18 100×2.1 mm×2.6 µm (**A**) and Kinetex Biphenyl 100×2.1 mm×1.7 µm (**B**) with MeOH as organic solvent.

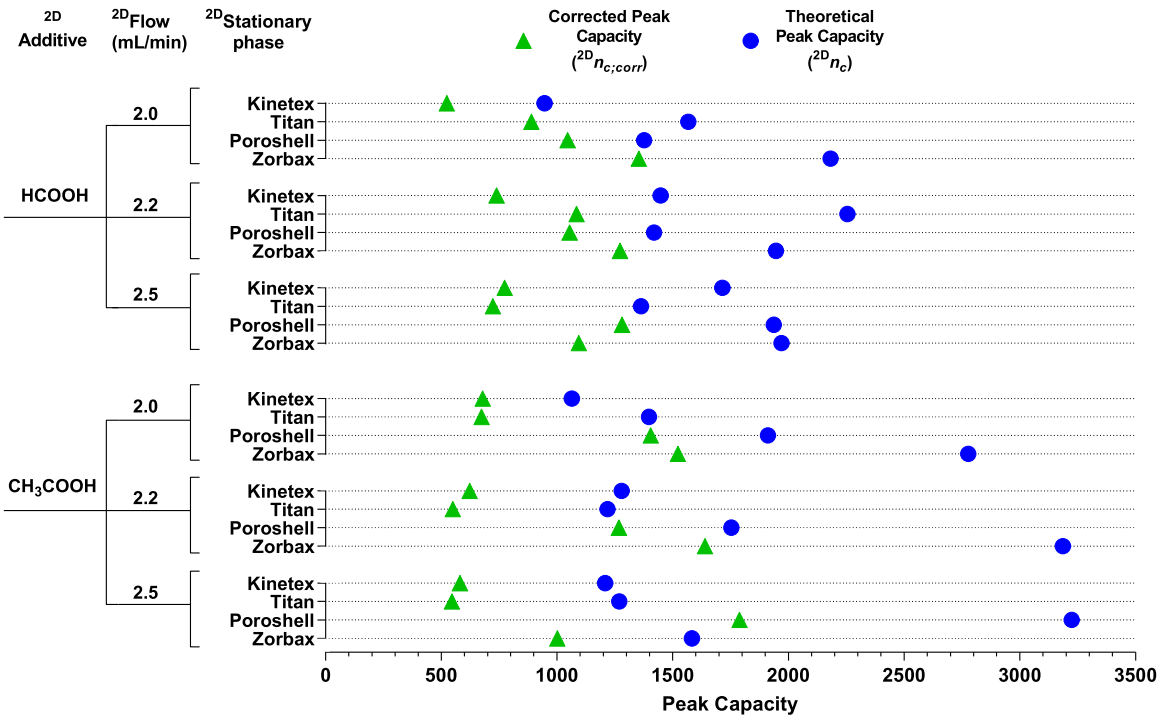

Fig. 2. Graph illustrating the comparison of peak capacities in 2D-LC using different additives (HCOOH and CH_3COOH), ^{2}D-flow rates (2.0, 2.2, and 2.5 mL/min), and ^{2}D-stationary phases (Kinetex, Titan, Poroshell, Zorbax). The symbols denote three types of peak capacity: theoretical (●), effective (■), and corrected (▲). This visualization highlights the influence of operational parameters on chromatographic performance.

combination of the ^{1}D separation using the Biphenyl column, combined with a ^{2}D separation on the superficially porous InfinityLab Poroshell 120 Bonus-RP 2.7 μm column showed the best corrected peak capacity ($2Dn_{c,corr}$) results, by using a flow rate of 2.5 and with solvent composition consisting of H_2O (0.1 % acetic acid, solvent A) and ACN (0.1 % acetic acid, solvent B). In these conditions, and considering the correction for the orthogonality (A_0), a $2Dn_{c,corr}$ valueof 1789 was achieved, which was higher than ZORBAX RRHD Eclipse Plus C18 ($2Dn_{c,corr}$ = 1002), Kinetex C18 ($2Dn_{c,corr}$ = 581), Titan C18 ($2Dn_{c,corr}$ = 546).

3.3. Choice of shifted gradient mode

The employment of a shifted gradient mode was considered where the percentage of organic solvent is adjusted based on the properties of the eluted fraction. This method proves to be particularly effective in RP × RP separations, enhancing peak distribution across the 2D space [31, 32].

Fig. 3 illustrates three different gradient separation modes for ^{2D}LC: full gradient mode (Fig. 3**A**), driven shift gradient mode (Fig. 3**B**), and segmented shift gradient mode (Fig. 3**C**). Among these, the Poroshell column operated with a segmented gradient (Fig. 3**C**) outperformed the other modes and column combinations, resulting in the highest values of orthogonality (A_0 = 71 %) and thus *corrected* peak capacity ($2Dn_{c,corr}$ = 1789). In this mode, the initial ratio was tailored to match the elution strength of the 1D mobile phase, while the gradient span was optimized based on the chemistry of the various compounds. This approach ensured that compounds with low retention in ^{1}D are effectively focused on the top of ^{2}D column, while strongly retained analytes were efficiently eluted, resulting in the optimal use of the entire 2D separation space. Regarding the steepness of the organic modifier gradient, various ramp profiles were evaluated to achieve a balance among the multiple compound classes present in the extract. For the final gradient conditions at longer 2D retention times, a higher organic content was selected to mitigate potential wrap-around effects in strongly retained compounds and to minimize column carryover of hydrophobic species.

Consequently, the segmented gradient mode proved to be the most suitable for separating and eluting the complex chemical components present in the *Allium cepa* leaf extract. This combination represents the optimal strategy for maximizing the 2D separation space, effectively combining high orthogonality with elevated peak capacity. Notably, lower values of peak capacity and orthogonality applied to polyphenols analysis in food and natural products for an RP-LC × RP-LC system have reported, further confirming the effectiveness of the system [33]. Complete results for all parameters considered are reported in supplementary **Table S3**, and the 2D plots for each separation are included in the Supporting Information (**Figure S3-S26)**.

3.4. 2D-LC method validation

The precision of analytical platform was assessed by monitoring chromatographic peaks from *Allium cepa* leaf extract and five selected standards under optimized RP-LC×RP-LC conditions (see materials and methods 2.6). Intraday repeatability was evaluated by analyzing the extract and standards at three different times on the same day, while interday repeatability was assessed at three intervals after six days. The intra- and interday precisions for both retention time and peak area in both dimensions are presented in terms of the coefficient of variation (% CV) in **Tables S4**. For the precision assessment, the %CV of peak areas and retention times, in both dimensions, ranged from 0.02 to 11.50 %, well within the acceptable limit of ± 15 % for analytical methods [34].

3.5. Characterization of the Allium cepa leaf extracts

The contour plots at 280 and 330 nm, relative to the separation of the *Allium cepa* leaf extracts, are reported in Figs. 4**A** and **B,** respectively.

The online hyphenation of RP-LC×RP-LC with HRMS, was carried out with both ionization polarities, in separate runs. The approach significantly enhanced compound identification compared to conventional mono-dimensional analytical methods allowing the detection of approximately 585 bubbles. Through the integration of different data

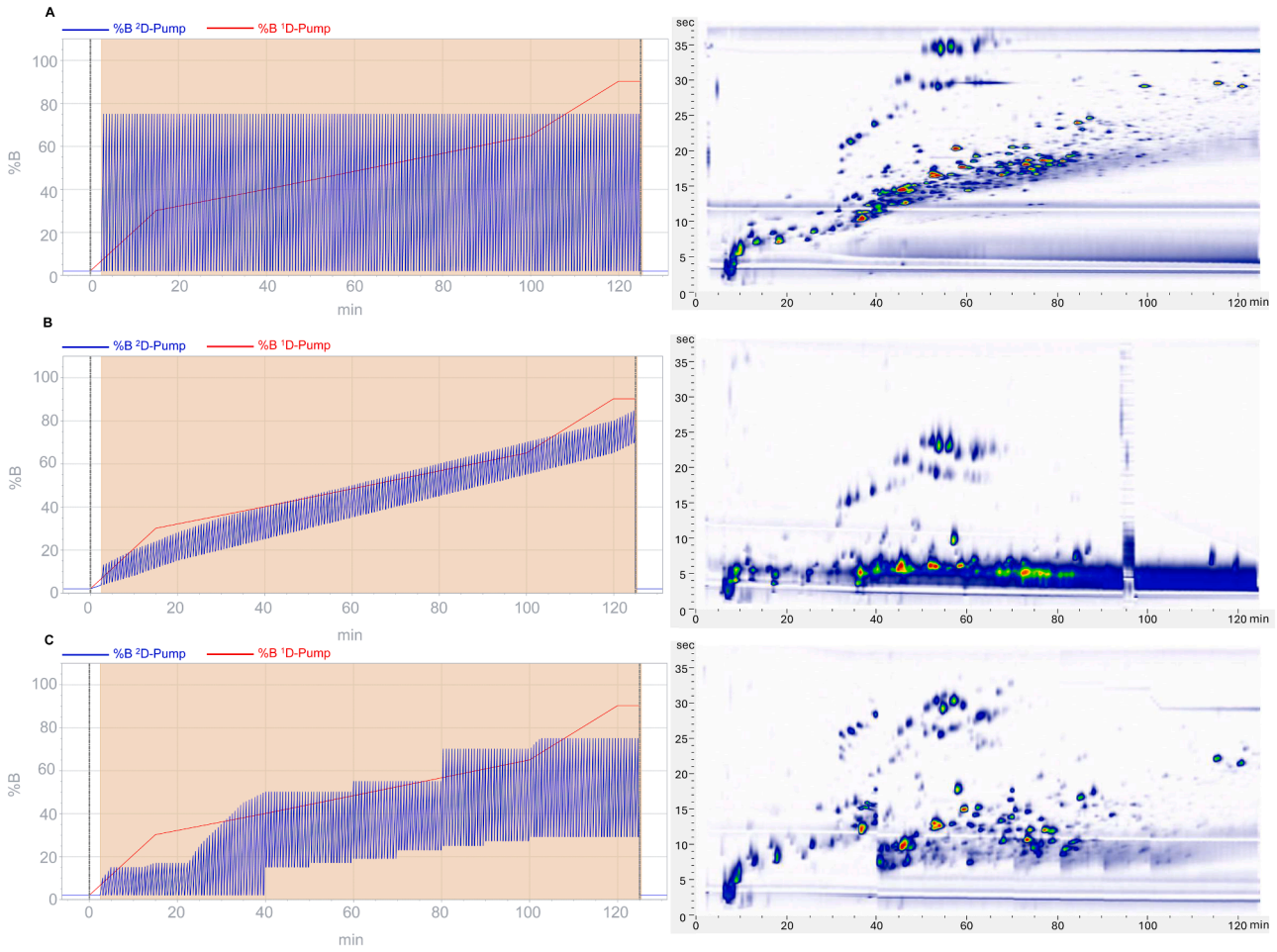

Fig. 3. Comparison of different gradient modes for ^{2D}LC: full gradient (**A**); driven shift gradient (**B**); segmented shift gradient mode (**C**). The red line corresponds to gradient profile in ^{1}D, and the blue line corresponds to gradient profile in ^{2}D.

analysis tools, such as Compound Discoverer and MZmine, a total of 147 analytes were tentatively identified: 110 analytes in negative and 37 compounds in positive ionization mode (see Supporting Information **Table S5**).

The analysis allowed us to confirm the presence of the compounds identified in the previous mono-dimensional analysis (64 compounds tentatively identified) [13] but revealed additional information on the chemical classes present, such as phenylpropanoids, isoprenoids, terpenes, dipeptides, further enriching the previously identified chemical classes including flavonoids, saponins, fatty acids, and lipids. A detailed 2D plot illustrating the distribution of classes across a two-dimensional space is presented in **Figure S27**.

3.5.1. Flavonoids

RP-LC×RP-LC—HRMS analysis confirmed that flavonoids, particularly flavonoid glycosides, represent the most abundant class of secondary metabolites, with kaempferol and quercetin identified as the predominant aglycones.

Among these, the compound with the highest peak value (83.66) was quercetin 3-(6″-feruloylsophorotrioside) (blob **1**). This compound had been previously identified in the mono-dimensional analysis, characterized by a $[M-H]^-$ ion at m/z 963 and a distinctive fragmentation pattern. The fragmentation involved the sequential loss of three sugar moieties (162 Da each), yielding the aglycone ion at m/z 300, along with the loss of a feruloyl moiety (176 Da), corresponding to the ion at m/z 787 (**Figure S28**) [13,35]. A similar fragmentation pattern was identified for **blob 9**, which displayed three main fragment ions at m/z 801 $[M-H-162]^-$, 625 $[M-H-162-176]^-$, and 301 $[M-H-162-176-162-162]^-$. These ions correspond to the sequential loss of a hexosyl residue, a ferulic group, and two additional sugar residues. This distinctive fragmentation pattern allowed for the tentative identification of compound 9 as a structural isomer of quercetin 3-(6″-feruloylsophorotrioside), also known as allivictoside H [36].

Another flavonoid glycoside, identified with quercetin as its aglycone, has been tentatively assigned to blob **312** (**Figure S29**). This compound exhibited a precursor ion at m/z 977, with fragment ions at m/z 609, corresponding to the loss of a sinapoyl group (206 Da), and at m/z 447, representing the loss of a hexoside moiety (162 Da), which corresponds to the loss of an additional hexosyl residue. A further fragment ion at m/z 301 reflected the loss of rhamnose, yielding the quercetin aglycone. The compound was ultimately annotated as quercetin 3-(6″- (E)-sinapylsophoroside)−7-rhamnoside.

The coupling with high resolution mass spectrometry enabled the elucidation of fragmentation patterns, such as that of rhamnazin 3-sophoroside (blob **41, Figure S30**). The $[M-H]^-$ ion at m/z 653, corresponding to the molecular formula $C_{29}H_{34}O_{17}$, produced fragment ions at m/z 621, 459, and 328. These fragments were attributed to the loss of a methoxyl group (32 Da) and the sequential loss of sugar residues (162 Da), respectively. The ion at m/z 328 provided structural insights into an O-methylated flavonol aglycone, such as rhamnazin. Additional minor fragments were observed at m/z 297 and 267, resulting from the further loss of methoxyl groups (32 Da).

Blob **2** could be annotated as kaempferol 3- [2″- (E) -feruloylsophoroside] −7-glucoside with its precursor ion at m/z 949 $[M+H]^+$. Fragment ion at m/z 339 could be used as diagnostic ions for the presence of feruloyl glucoside group (176+162 Da). Furthermore,

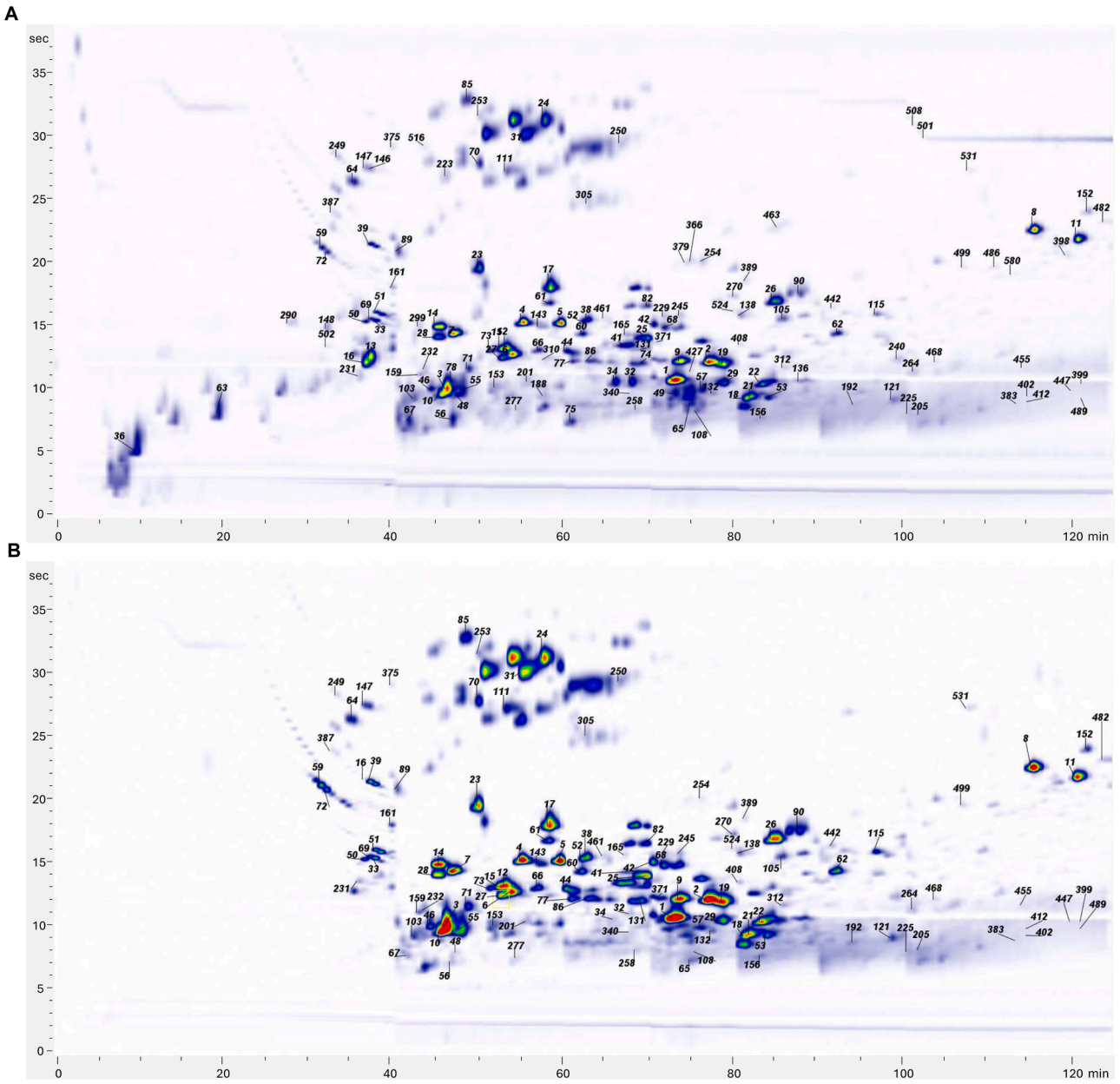

Fig. 4. 2D LC×LC plot of *Allium cepa* leave extract at 280 nm (**A**) and 330 nm (**B**). ^{1}D column: Kinetex Biphenyl 100×2.1 mm×1.7 μm; ^{2}D column: InfinityLab Poroshell 120 Bonus-RP column 3.0 × 50 mm×2.7 μm. For MS Peak identification, see Supporting Information **Table S5**.

aglycone fragment ion at m/z 287 was produced after the loss of feruloyl glucoside moiety and sophoroside residue (162+162 Da) (**Figure S31**) [13,37].

As shown in **Figure S32**, compound **21** exhibited a precursor ion at m/z 919 $[M + H]^+$, corresponding to the molecular formula $C_{42}H_{46}O_{23}$. MS/MS spectra revealed key fragment ions, including m/z 287 ($C_{15}H_{11}O_6$), attributed to the kaempferol aglycone, and m/z 309 ($C_{15}H_{17}O_7$), associated with the coumaroyl glycoside residue. Additionally, fragment ions at m/z 165 ($C_9H_9O_3$) and m/z 147 ($C_9H_7O_2$) confirmed the existence of the coumaroyl group. According to MS/MS fragmentation pattern, compound 21 was tentatively identified as allivictoside E (kaempferol-3-*O*-coumaroyl diglucoside-7-*O*-glucoside) [13, 36].

3.5.2. Coumestans

Among the flavonoids, coumestans such as demethylwedelolactone (blob **15**) have also been tentatively identified, with a precursor ion $[M + H]^+$ at m/z 301 in positive ion mode, corresponding formula to $C_{15}H_8O_7$. Compound **15** exhibited a typical fragmentation behavior for coumarins (**Figure S33**) [38,39] with the loss of CO or CO_2 from the ester group, resulting in ions at m/z 273 and 255, respectively. On the other hand, a subsequent loss of CO in phenol group for m/z 273 results in a product ion at m/z 245 $[M + H—CO—CO]^{+1}$.

3.5.3. Chalcones

Another class of chemical compounds identified in the extract comprises chalcones, represented by phloretin 3′,5′-Di-C-glucoside (blob **86**) and 4-methoxyphlorizin (blob **131**).

Both compounds exhibited similar negative ion MS/MS fragmentation patterns (**Figure S34**). Compound **86** displayed a precursor ion $[M-H]^-$ at m/z 597 ($C_{27}H_{34}O_{15}$), while compound **131** showed a precursor ion at m/z 449 ($C_{22}H_{26}O_{10}$). Characteristic ions at m/z 435 and 273 indicated the presence of phlorizin ($C_{21}H_{24}O_{10}$) and phloretin aglycone ($C_{15}H_{14}O_5$), respectively. Furthermore, the presence of carbonyl group

at C-3′ position facilitated cleavage of C2'−3′ bond, generating ions at m/z 167 and 181 for compound **86** and **131**, respectively [40–42].

3.5.4. Isoprenoids

The ^{2}D-HRMS/MS analysis also enabled the identification of isoprenoids and phenylpropanoids. Feruloyl loganic acid (blob **310**) was tentatively identified based on its precursor ion $[M-H]^-$at m/z 551. The fragment ion at m/z 389 resulted from the neutral loss of a glucose moiety ($[M-H-162]^-$). The product ion at m/z 341 was formed by the combined loss of H_2O/HCHO (48 Da) [43]. Fragment ions at m/z 195 and m/z 193 suggested the cleavage of the C7–7″ bond, indicating the presence of a deoxyloganetic acid unit linked to a unit derived from ferulic acid [44,45]. Additional ions (m/z 178, 165, 149, 134), characteristic of the ferulic acid fragmentation pattern, were observed (**Figure S35**).

3.5.5. Hydroxycinnamic acids

Blob **138** (**Figure S36**) was tentatively identified as N-*trans*-feruloyltyramine ($[M+H]^+$, m/z 314). The mass fragmentation analysis showed two major daughter ions which could be attributed to the hydroxycinnamic subunit m/z 194 (ferulic amide) and m/z 177 (ferulic aldehyde) [46]. Additionally, a mass difference of 30 Da (m/z 145) from the ferulic aldehyde ion suggested the loss of a methoxy group (OCH_3–), while m/z 121 indicated the presence of a 4-ethylphenol residue [47]. The presence of an additional methoxy group ($[M+H]^+$, m/z 344) and a similar fragmentation pattern led to the tentative identification of N-*trans*-feruloyl-3-methoxytyramine (blob **105**) [48].

3.5.6. Saponins

According to the negative fragmentation pattern, blobs **121, 225** and **264** were tentatively identified as isomers of ceposide C, exhibiting a molecular ion $[M-H]^-$at m/z 917 ($C_{45}H_{74}O_{19}$). In MS2 spectra, these compounds displayed fragment ions at m/z 771 and m/z 609, corresponding to the losses of a deoxyhexosyl (146 Da) and a hexosyl (162 Da) moieties, respectively. Further cleavage of an additional hexosyl moiety yielded the sapogenin deprotonated ion at m/z 447 (**Figure S37**).

A similar fragmentation pattern was observed for blob **53** ($[M-H]^-$, m/z 919, $C_{45}H_{76}O_{19}$), which also showed sequential losses of a deoxyhexosyl (146 Da) and two hexosyl (324 Da) moieties, ultimately producing the sapogenin deprotonated ion at m/z 449.

Ceposide A and B were also tentatively identified (blobs **383** and **455**). These molecules differ from ceposide C by the presence of an additional pentosyl residue (132 Da) in place of a hexosyl residue. In their fragmentation patterns, they similarly produced the deprotonated sapogenin ion at m/z 447, following the sequential losses of a deoxyhexosyl group (at m/z 741), a hexosyl moiety (m/z 579), and finally a pentosyl residue (m/z 447).

3.5.7. Fatty acids and lipids

Fatty acids were identified both in positive and negative ionization modes. Based on the negative fragmentation patterns, it was possible to tentatively identify fatty acids belonging to the subclasses of monocarboxylic (MFA) and dicarboxylic (DFA) fatty acids. Generally, their fragmentation pattern corresponds to the neutral loss of water moiety (18 Da) and/or CO_2 (44 Da). Among DFA, azelaic acid (blob **165** and **371**) was putatively identified by the deprotonated molecular ion at m/z 187 $[M-H]^-$, which produced fragment ions at m/z 169 $[M-H-H_2O]^-$, m/z 143 $[M-H-CO_2]^-$, and m/z 125 $[M-H-CO_2-H_2O]^-$ (**Figure S38**).

Blobs **499** and **531** were tentatively identified as trihydroxyoctadecenoic acid (FA 18:1;O3) isomers, which belong to MFA subclass. This identification was corroborated by the detection of the deprotonated molecular ion at m/z 329, along with a base fragment peak at m/z 311, which resulted from the loss of a water molecule. Additional fragment ions at m/z 293, m/z 229, and m/z 211 were observed, likely resulting from the loss of aliphatic groups.

ESI positive analysis highlighted the presence of fatty acid amides (FAA) and sphingolipids. In addition to stearamide (blob **156**), palmitoleamide (blob **392**), dehydrosphingosine (blob **489**) and sphingosine (blob **501**), which had already been identified in the mono-dimensional previously analyses, the presence of fatty acid amides (FAA) such as linoleamide (blob **253**), erucamide (blob **280**), myristamide (blob **331**), lauramide (blob **393**), and oleamide (blob **398**) was also detected.

These peaks were tentatively identified as $[M+H]^+$ ions, showing diagnostic fragments ions in the MS/MS spectra corresponding to the cleavage of acyl chains: m/z 116.1123 $[C_6H_{14}NO]^+$, m/z 102.0897 $[C_5H_{12}NO]^+$, m/z 88.0739 $[C_4H_{10}NO]^+$, and m/z 74.0631 $[C_3H_8NO]^+$[49] (**Figure S39**).

3.6. Antioxidant power evaluation by pre-column DPPH reaction coupled to LC × LC platform

The DPPH assay is based on the reaction between the DPPH radical (DPPH•) and antioxidants, resulting in a reduction in absorbance as the radical is neutralized (DPPH—H). A hallmark of this reaction is the color change from purple (DPPH•) to yellow (DPPH—H). Antioxidant capacity is quantified by measuring the absorbance difference of the DPPH radical solution before and after its interaction with the antioxidant. While widely used, this assay alone cannot distinguish the individual contributions of specific analytes within a complex matrix. To address this limitation and accurately determine the contribution of individual compounds to the antioxidant activity in extracts from natural matrices, pre- and post-column derivatization techniques with DPPH coupled to HPLC have been effectively utilized [50–52]. By integrating separation techniques, as demonstrated by Tang et al. (2008), the assay allows the identification of each analyte's specific impact [53].

Over the years, researchers transitioned from the use of fully porous particle columns to approaches employing a core-shell C18 column in pre- [27,54] and post-column [55,56] DPPH techniques, achieving rapid separation with excellent chromatographic resolution. Clearly with very complex matrices, 1D-LC is still a bottleneck for the evaluation of potentially relevant antioxidant compounds and hence precolumn-DPPH LC × LC can be a viable alternative. Key factors influencing the method's effectiveness included the DPPH-to-extract ratio and reaction time. An excess DPPH resulted in the disappearance of all analyte peaks from the UV–Vis trace, making it impossible to distinguish antioxidant activity, while insufficient DPPH led to negligible differences. In this study, 5 mM DPPH was found to be optimal concentration. Concerning reaction time, after 30 min no further changes occurred, indicating stabilization and confirming the solution's stable yellow color.

The PDA chromatograms of before and after the pre-column DPPH reaction are reported in Fig. 5. By comparing the overlaid chromatograms of samples treated and untreated with the DPPH radical, it is evident that several peaks were significantly reduced, with only a few disappearing entirely.

Among compounds reported in Table 1, it can be observed that flavonoids, isoprenoids, and phenylpropanoids are the main classes involved in the antioxidant activity (> 50 %), as confirmed by previous studies [57–60]. This can primarily be attributed to their molecular structures, which contain multiple hydroxyl groups, and thus responsible for the hydrogen atom transfer (HAT) mechanisms and/or as SET (single electron transfer) and SPLET (sequential proton loss electron transfer) that might neutralize DPPH• radical [61,62].

The compound with the highest antioxidant power (RSA: 91.32 ± 4.18 %) was found to be phloretin 3′,5′-di-C-glucoside (blob **86**). Specifically, the relationship between the antioxidant activities and chemical structures of chalcones has been extensively analyzed [63–65]. To support these findings, it is worth highlighting the contribution to antioxidant activity of other chalcones as well, such as 4-methoxyphlorizin (RSA: 79.25 ± 3.58 %) (blob **131**). Together with phloretin 3′, 5′-di-C-glucoside, these compounds represent glycosylated derivatives of

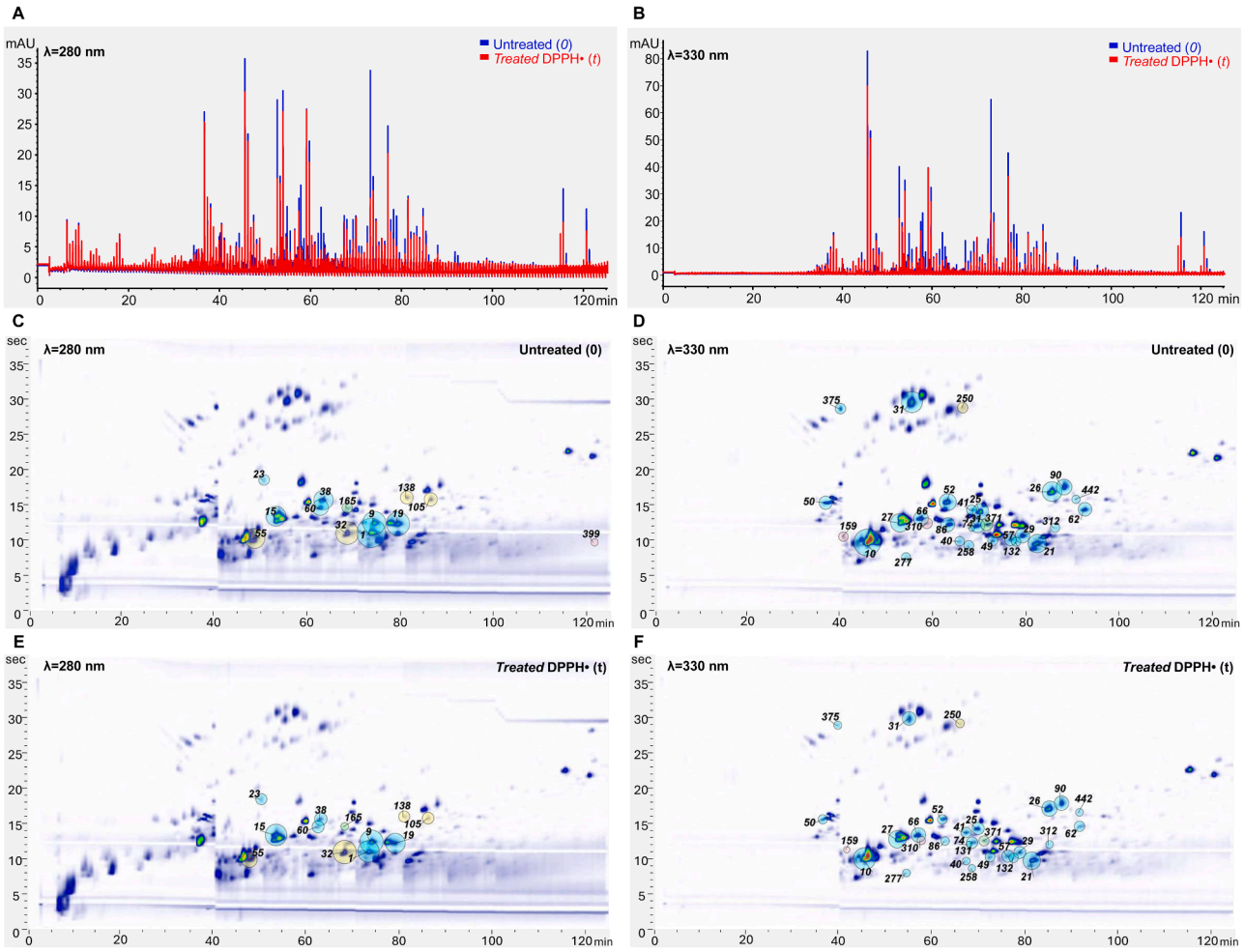

Fig. 5. Overlapped DPPH- LC×LC-DAD chromatograms of *Allium cepa* leaf extract at 280 nm (**A**) and 330 nm (**B**), comparing untreated (0) extract and treated (*t*) extract with DPPH•. 2D plots of compounds are shown for untreated (0) e and treated (*t*) samples at 280 nm (**C** and **E**) and 330 nm (**D** and **F**). These visualizations highlight the impact of DPPH radical treatment on the chemical profile of the extract.

phloretin, whose antioxidant capacities were studied by Mendes, R.A. et al. (2018) [66].

Moreover, as described in numerous studies, flavonoids such as myricetin and quercetin, which have a more hydroxylated B ring, contribute significantly to the mechanism of protection against oxidative stress [67,68]. On this matter, the peaks most associated in the quenching of the radical in the *Allium cepa* leaf extract correspond to flavonoids that have as main aglycone quercetin. For example, allivictoside H (blob **9**) exhibited a RSA value of 79.10 ± 4.64 %, while quercetin 3- (6″- (E) -sinapylsophoroside) −7-rhamnoside (blob **312**) demonstrated an RSA of 78.24 ± 3.29 %.

Feruloyl loganic acid (blob **310**) was identified as the isoprenoid compound most involved in the radical-scavenging activity of the extract (RSA: 84.29 ± 6.68 %). Isoprenoids, along with phenylpropanoids, have been extensively studied for their antioxidant properties [69,70]. Concerning phenylpropanoids Lopez-Munguia, A. et al. (2011) reported a study on the antioxidant activity of phenylpropanoid glycosides (PPGs), demonstrating a better antiradical activity of PPGs when compared to their phenylpropanoid precursor or alcohol derivatives [71]. N-trans-Feruloyl-tyramine (blob **138**) exhibited a RSA value of 81.79 ± 1.72 %, making it the most active phenylpropanoid in the *Allium cepa* leaf extract.

4. Conclusion

In this contribution, the development and optimization of highly efficient RP-LC×RP-LC-PDA-HRMS platform has demonstrated significant potential in analyzing complex matrices, such as *Allium cepa* PDO leaves extracts. The RP-LC×RP-LC method, coupled with high-resolution mass spectrometry (HRMS), enabled the detailed characterization of 147 compounds distributed across a wide range of chemical classes, including flavonoids, saponins, phenylpropanoids, isoprenoids, terpenes, dipeptides, fatty acids, and lipids. This chemical diversity underscores the potential of *Allium cepa* leaves as a rich source of bioactive compounds. The in-depth profiling was achieved using an optimized workflow: the ^{1}D separation was performed on a core-shell Kinetex Biphenyl column (100×2.1 mm×1.7 μm), while the ^{2}D separation employed a superficially porous InfinityLab Poroshell 120 Bonus-RP column (50×3.0 mm ×2.7 μm). This configuration maximized the utilization of the ^{2}D separation space, significantly enhancing separation efficiency while overcoming limitations associated with conventional mono-dimensional methods. Moreover, antioxidant activity analysis, performed by a pre-column DPPH-LC×LC-DAD analysis, revealed 50 key molecules exhibited radical scavenging activity above 50 %, with the majority belonging to the classes of flavonoids, isoprenoids, and phenylpropanoids. The developed methodologies underscore the importance of two-dimensional chromatography techniques for valorizing agricultural by-products, enabling detailed characterization of secondary metabolites and the standardization of biomarkers with antioxidant properties. These approaches provide valuable contributions to industrial applications in the food and pharmaceutical sectors, promoting a sustainable strategy to manage agricultural by-products by transforming

Table 1
Contribution of single compounds to the antioxidant activity by DPPH- LC × LC-DAD method.

Blob ID	λ (nm)	Rt (min)	Compound Name	Class	RSA (%)
86	330	62.99	Phloretin 3′,5′-di-C-glucoside	Flavonoids	91.32 ± 4.18
310	330	57.87	Feruloyl loganic acid	Isoprenoid	84.29 ± 6.68
138	280	80.96	N-trans-Feruloyl-tyramine	Phenylpropanoids	81.79 ± 1.72
131	330	69.40	4-Methoxyphlorizin	Flavonoids	79.25 ± 3.58
9	280	73.87	Allivictoside H	Flavonoids	79.10 ± 4.64
312	330	86.02	Quercetin 3- (6″- (E) -sinapylsophoroside) −7-rhamnoside	Flavonoids	78.24 ± 3.29
258	330	68.68	Isoliquiritigenin 2′-glucosyl- (1->4) -rhamnoside	Flavonoids	78.19 ± 1.42
132	330	77.66	2′,4′-Dihydroxy-3′,6′-dimethoxydihydrochalcone 4′-gentiobioside (Salicifolioside A)	Flavonoids	76.41 ± 0.29
52	330	62.40	Myricetin 3,3′-digalactoside	Flavonoids	76.03 ± 7.80
442	330	91.76	Quercetin 3- (2″-feruloylsophoroside)	Flavonoids	75.13 ± 3.42
32	280	68.08	Syringaresinol glucoside (tortoside A o Acanthoside B)	Monolignol and oligolignol	74.98 ± 5.23
250	330	67.11	Methylsyringin	Phenolic glycosides	74.63 ± 6.26
15	280	52.76	Demethylwedelolactone	Flavonoids	72.83 ± 6.68
10	330	45.66	Kaempferol-3-O-sophoroside-7-O-d-glucoside	Flavonoids	72.31 ± 9.37
21	330	82.14	Allivictoside E (Kaempferol-3-O-coumaroyl diglucoside-7-O-glucoside)	Flavonoids	72.09 ± 4.72
62	330	92.46	Quercetin 3- (2″-feruloylsophoroside)	Flavonoids	70.88 ± 2.57
38	280	63.04	Myricitrin	Flavonoids	70.78 ± 7.16
60	280	62.38	Quercetin 3,4′-di-O-beta-d-glucopyranoside	Flavonoids	70.71 ± 2.75
23	280	58.60	Quercetin-3-O-βD-glucopyranoside (Isoquercetin)	Flavonoids	70.22 ± 1.02
159	330	43.13	Monoterpenols pentosyl-hexoside (linalool/geraniol isomer hexose-pentose)	Isoprenoids	69.63 ± 6.56
41	330	67.49	Rhamnazin 3-sophoroside	Flavonoids	69.55 ± 4.72
74	330	69.38	Quercetin-3-O- sophoroside-7-O-feruloyl-diglucoside	Flavonoids	69.49 ± 8.42
375	330	40.22	8-Hydroxytricetin 7-glucuronide	Flavonoids	68.34 ± 3.45
55	280	48.23	Sinapic acid glucose	Phenylpropanoids	66.81 ± 0.54
50	330	36.80	Syringic acid-4-beta-d-glucopyranoside	Flavonoids	66.79 ± 4.91
90	330	88.03	7-Hydroxy-2′,4′,5-trimethoxyflavanone	Flavonoids	66.50 ± 8.01
49	330	73.19	Quercetin 3-[2′′′-(E)-caffeylsophoroside]−7-glucoside	Flavonoids	65.04 ± 2.82
340	330	68.06	Flavaprin	Flavonoids	64.02 ± 4.87
27	330	52.75	Quercetin 3,4′-di-O-beta-d-glucopyranoside	Flavonoids	62.59 ± 7.54
371	330	71.33	Nonanedioic acid (Azelaic acid)	Dicarboxylic fatty acid	61.92 ± 7.9
31	330	55.60	Ellagic acid acetyl-arabinoside	Phenylpropanoids	61.19 ± 8.78
277	330	54.60	Cyanidin 3-laminaribioside	Flavonoids	60.93 ± 6.73
399	280	121.20	3-Methoxyacetophenone	Isoprenoids	60.36 ± 2.00
26	330	84.82	Trimethoxyflavone	Flavonoids	60.26 ± 0.64
29	330	78.96	6-Hydroxyluteolin-7- (6″-caffeylsophoroside)	Flavonoids	59.46 ± 0.73
1	280	73.20	Quercetin 3- (6‴-ferulylsophorotrioside)	Flavonoids	58.89 ± 4.22
66	330	57.24	Isorhamnetin-3-Oβ-gentiobioside	Flavonoids	58.50 ± 2.91
57	330	76.39	Allyltetramethoxybenzene	Benzenoids	57.88 ± 5.18
19	280	78.98	Quercetin-3-O-coumaroyl-sophoroside-7-O-d-glucoside	Flavonoids	56.28 ± 1.42
165	280	67.50	Nonanedioic acid (Azelaic acid)	Dicarboxylic fatty acid	51.00 ± 7.31
25	330	70.06	Quercetin-3-O-coumaroyl-sophoroside-7-O-d-glucoside	Flavonoids	50.68 ± 10.74
105	280	86.08	N-trans-Feruloyl-3-methoxytyramine	Phenylpropanoids	50.53 ± 9.47

*Data are expressed as mean ± standard deviation ($n = 2$).

them into high-value-added resources.

CRediT authorship contribution statement

Giovanna Aquino: Writing – original draft, Formal analysis. **Eduardo Maria Sommella:** Supervision. **Emanuela Salviati:** Data curation. **Michele Manfra:** Writing – review & editing. **Giulia Auriemma:** Writing – review & editing. **Pietro Campiglia:** Funding acquisition. **Giacomo Pepe:** Supervision. **Manuela Giovanna Basilicata:** Data curation.

Declaration of competing interest

The authors declare the following financial interests/personal relationships which may be considered as potential competing interests:

Pietro Campiglia reports was provided by Government of Italy Ministry of Education University and Research.

Acknowledgments

This study was carried out within the Agritech National Research Center and received funding from the European Union Next-GenerationEU (PIANO NAZIONALE DI RIPRESA E RESILIENZA (PNRR) – MISSIONE 4 COMPONENTE 2, INVESTIMENTO 1.4 – D.D. 1032 17/06/2022, CN00000022). This manuscript reflects only the authors' views and opinions, neither the European Union nor the European Commission can be considered responsible for them. This work was also supported by Ministero dell'Università e della Ricerca (MIUR) project PIR01_00032 BIO OPEN LAB BOL "CUP" J37E19000050007, project CIR01_00032 – BOL "BIO Open Lab—Rafforzamento del capitale umano", project "Pathogen Readiness Platform for CERIC ERIC upgrade"—PRP@CERIC CUP J97G22000400006.

Supplementary materials

Supplementary material associated with this article can be found, in the online version, at doi:10.1016/j.chroma.2025.465877.

Data availability

Data will be made available on request.

References

[1] A. Nayak, B. Bhushan, An overview of the recent trends on the waste valorization techniques for food wastes, J. Environ. Manage 233 (2019) 352–370, https://doi.org/10.1016/j.jenvman.2018.12.041.
[2] K. Kumar, A.N. Yadav, V. Kumar, P. Vyas, H.S. Dhaliwal, Food waste: a potential bioresource for extraction of nutraceuticals and bioactive compounds, Bioresour. Bioprocess. 4 (1) (2017) 18, https://doi.org/10.1186/s40643-017-0148-6.
[3] A. Mir-Cerdà, O. Nuñez, M. Granados, S. Sentellas, J. Saurina, An overview of the extraction and characterization of bioactive phenolic compounds from agri-food

waste within the framework of circular bioeconomy, TrAC Trend. Anal. Chem. 161 (2023) 116994, https://doi.org/10.1016/j.trac.2023.116994.
[4] E. Tammekivi, C. Geantet, C. Lorentz, K. Faure, Two-dimensional chromatography for the analysis of valorisable biowaste: a review, Anal. Chim. Acta 1283 (2023) 341855, https://doi.org/10.1016/j.aca.2023.341855.
[5] G. La Barbera, A.L. Capriotti, C. Cavaliere, C.M. Montone, S. Piovesana, R. Samperi, R. Zenezini Chiozzi, A. Laganà, Liquid chromatography-high resolution mass spectrometry for the analysis of phytochemicals in vegetal-derived food and beverages, Food Res. Int. 100 (2017) 28–52, https://doi.org/10.1016/j.foodres.2017.07.080.
[6] P. Donato, F. Cacciola, P.Q. Tranchida, P. Dugo, L. Mondello, Mass spectrometry detection in comprehensive liquid chromatography: basic concepts, instrumental aspects, applications and trends, Mass Spectrom. Rev. 31 (5) (2012) 523–559, https://doi.org/10.1002/mas.20353.
[7] F. Cacciola, F. Rigano, P. Dugo, L. Mondello, Comprehensive two-dimensional liquid chromatography as a powerful tool for the analysis of food and food products, TrAC Trend. Anal. Chem. 127 (2020) 115894, https://doi.org/10.1016/j.trac.2020.115894.
[8] E. Lazzari, K. Arena, E.B. Caramão, P. Dugo, L. Mondello, M. Herrero, Comprehensive two-dimensional liquid chromatography-based quali-quantitative screening of aqueous phases from pyrolysis bio-oils, Electrophoresis 42 (1–2) (2021) 58–67, https://doi.org/10.1002/elps.202000119.
[9] E. Sommella, G. Pepe, G. Ventre, F. Pagano, M. Manfra, G. Pierri, O. Ismail, A. Ciogli, P. Campiglia, Evaluation of two sub-2μm stationary phases, core–shell and totally porous monodisperse, in the second dimension of on-line comprehensive two dimensional liquid chromatography, a case study: separation of milk peptides after expiration date, J. Chromatogr. A 1375 (2015) 54–61, https://doi.org/10.1016/j.chroma.2014.11.072.
[10] T. Brazdauskas, L. Montero, P.R. Venskutonis, E. Ibañez, M. Herrero, Downstream valorization and comprehensive two-dimensional liquid chromatography-based chemical characterization of bioactives from black chokeberries (Aronia melanocarpa) pomace, J. Chromatogr. A 1468 (2016) 126–135, https://doi.org/10.1016/j.chroma.2016.09.033.
[11] K.M. Kalili, J. Vestner, M.A. Stander, A. de Villiers, Toward unraveling grape tannin composition: application of online hydrophilic interaction chromatography × reversed-phase liquid chromatography–Time-of-flight mass spectrometry for grape seed analysis, Anal. Chem. 85 (19) (2013) 9107–9115, https://doi.org/10.1021/ac401896r.
[12] L. Montero, V. Sáez, D. von Baer, A. Cifuentes, M. Herrero, Profiling of Vitis vinifera L. canes (poly)phenolic compounds using comprehensive two-dimensional liquid chromatography, J. Chromatogr. A 1536 (2018) 205–215, https://doi.org/10.1016/j.chroma.2017.06.013.
[13] G. Aquino, M.G. Basilicata, C. Crescenzi, V. Vestuto, E. Salviati, M. Cerrato, T. Ciaglia, F. Sansone, G. Pepe, P. Campiglia, Optimization of microwave-assisted extraction of antioxidant compounds from spring onion leaves using Box–Behnken design, Sci. Rep. 13 (1) (2023) 14923, https://doi.org/10.1038/s41598-023-42303-x.
[14] B.W.J. Pirok, A.F.G. Gargano, P.J. Schoenmakers, Optimizing separations in online comprehensive two-dimensional liquid chromatography, J. Sep. Sci. 41 (1) (2018) 68–98, https://doi.org/10.1002/jssc.201700863.
[15] X. Li, D.R. Stoll, P.W. Carr, Equation for peak capacity estimation in two-dimensional liquid chromatography, Anal. Chem. 81 (2) (2009) 845–850, https://doi.org/10.1021/ac801772u.
[16] J.M. Davis, Dependence of effective peak capacity in comprehensive two-dimensional separations on the distribution of peak capacity between the two dimensions, Anal. Chem. 80 (21) (2008) 8122–8134, https://doi.org/10.1021/ac800933z.
[17] H. Gu, Y. Huang, P.W. Carr, Peak capacity optimization in comprehensive two dimensional liquid chromatography: a practical approach, J. Chromatogr. A 1218 (1) (2011) 64–73, https://doi.org/10.1016/j.chroma.2010.10.096.
[18] H. Gu, Y. Huang, M. Filgueira, P.W. Carr, Effect of first dimension phase selectivity in online comprehensive two dimensional liquid chromatography (LC×LC), J. Chromatogr. A 1218 (38) (2011) 6675–6687, https://doi.org/10.1016/j.chroma.2011.07.063.
[19] J.M. Davis, D.R. Stoll, P.W. Carr, Effect of first-dimension undersampling on effective peak capacity in comprehensive two-dimensional separations, Anal. Chem. 80 (2) (2008) 461–473, https://doi.org/10.1021/ac071504j.
[20] M. Gilar, P. Olivova, A.E. Daly, J.C. Gebler, Orthogonality of separation in two-dimensional liquid chromatography, Anal. Chem. 77 (19) (2005) 6426–6434, https://doi.org/10.1021/ac050923i.
[21] M. Gilar, J. Fridrich, M.R. Schure, A. Jaworski, Comparison of orthogonality estimation methods for the two-dimensional separations of peptides, Anal. Chem. 84 (20) (2012) 8722–8732, https://doi.org/10.1021/ac3020214.
[22] S.C. Rutan, J.M. Davis, P.W. Carr, Fractional coverage metrics based on ecological home range for calculation of the effective peak capacity in comprehensive two-dimensional separations, J. Chromatogr. A 1255 (2012) 267–276, https://doi.org/10.1016/j.chroma.2011.12.061.
[23] M. Camenzuli, P.J. Schoenmakers, A new measure of orthogonality for multi-dimensional chromatography, Anal. Chim. Acta 838 (2014) 93–101, https://doi.org/10.1016/j.aca.2014.05.048.
[24] L.W. Sumner, A. Amberg, D. Barrett, M.H. Beale, R. Beger, C.A. Daykin, T.W. M. Fan, O. Fiehn, R. Goodacre, J.L. Griffin, T. Hankemeier, N. Hardy, J. Harnly, R. Higashi, J. Kopka, A.N. Lane, J.C. Lindon, P. Marriott, A.W. Nicholls, M.D. Reily, J.J. Thaden, M.R. Viant, Proposed minimum reporting standards for chemical analysis, Metabolomics. 3 (3) (2007) 211–221, https://doi.org/10.1007/s11306-007-0082-2.
[25] R. Schmid, S. Heuckeroth, A. Korf, A. Smirnov, O. Myers, T.S. Dyrlund, R. Bushuiev, K.J. Murray, N. Hoffmann, M. Lu, A. Sarvepalli, Z. Zhang, M. Fleischauer, K. Dührkop, M. Wesner, S.J. Hoogstra, E. Rudt, O. Mokshyna, C. Brungs, K. Ponomarov, L. Mutabdžija, T. Damiani, C.J. Pudney, M. Earll, P. O. Helmer, T.R. Fallon, T. Schulze, A. Rivas-Ubach, A. Bilbao, H. Richter, L.-F. Nothias, M. Wang, M. Orešič, J.-K. Weng, S. Böcker, A. Jeibmann, H. Hayen, U. Karst, P.C. Dorrestein, D. Petras, X. Du, T. Pluskal, Integrative analysis of multimodal mass spectrometry data in MZmine 3, Nat. Biotechnol. 41 (4) (2023) 447–449, https://doi.org/10.1038/s41587-023-01690-2.
[26] C. Brungs, R. Schmid, S. Heuckeroth, A. Mazumdar, M. Drexler, P. Šácha, P.C. Dorrestein, D. Petras, L.-F. Nothias, V. Veverka, Efficient generation of open multi-stage fragmentation mass spectral libraries, (2024). 10.26434/chemrxiv-2024-l1tqh-v2.
[27] E. Sommella, G. Pepe, F. Pagano, G. Conte, F. Carimi, G.C. Tenore, E. Novellino, M. Manfra, M. Russo, P. Campiglia, Rapid screening of antioxidant anthocyanins in autochthonous Nero d'Avola grape clones by pre-column DPPH reaction coupled to UHPLC-UV/vis-IT-TOF: a strategy to combine chemical data and genetic diversity, Food Anal. Methods 9 (10) (2016) 2780–2790, https://doi.org/10.1007/s12161-016-0472-z.
[28] L. Mondello, P. Dugo, P. Donato, M. Herrero, L. Montero, O.J. Schmitz, Comprehensive two-dimensional liquid chromatography, Nat. Rev. Method. Primers 3 (1) (2023) 86, https://doi.org/10.1038/s43586-023-00269-0.
[29] E. Sommella, O.H. Ismail, F. Pagano, G. Pepe, C. Ostacolo, G. Mazzoccanti, M. Russo, E. Novellino, F. Gasparrini, P. Campiglia, Development of an improved online comprehensive hydrophilic interaction chromatography × reversed-phase ultra-high-pressure liquid chromatography platform for complex multiclass polyphenolic sample analysis, J. Sep. Sci. 40 (10) (2017) 2188–2197, https://doi.org/10.1002/jssc.201700134.
[30] M. Yang, S. Fazio, D. Munch, P. Drumm, Impact of methanol and acetonitrile on separations based on π–π interactions with a reversed-phase phenyl column, J. Chromatogr. A 1097 (1) (2005) 124–129, https://doi.org/10.1016/j.chroma.2005.08.028.
[31] S. Chapel, F. Rouvière, S. Heinisch, Sense and nonsense of shifting gradients in on-line comprehensive reversed-phase LC × reversed-phase LC, J. Chromatogr. B 1212 (2022) 123512, https://doi.org/10.1016/j.jchromb.2022.123512.
[32] D. Li, O.J. Schmitz, Use of shift gradient in the second dimension to improve the separation space in comprehensive two-dimensional liquid chromatography, Anal. Bioanal. Chem. 405 (20) (2013) 6511–6517, https://doi.org/10.1007/s00216-013-7089-5.
[33] F. Cacciola, K. Arena, F. Mandolfino, D. Donnarumma, P. Dugo, L. Mondello, Reversed phase versus hydrophilic interaction liquid chromatography as first dimension of comprehensive two-dimensional liquid chromatography systems for the elucidation of the polyphenolic content of food and natural products, J. Chromatogr. A 1645 (2021) 462129, https://doi.org/10.1016/j.chroma.2021.462129.
[34] F.a.D.A.U.S.D.o.H.a.H. Services, C.f.D.E.a.R. (CDER), C.f.V.M. (CMV), bioanalytical method validation: guidance for industry, (2018).
[35] A. Pineda, A. Arenas, J. Balmaceda, G.E. Zúñiga, Extracts of fruits and plants cultivated In vitro of Aristotelia chilensis (Mol.) Stuntz show inhibitory activity of aldose reductase and pancreatic alpha-amylase enzymes, Plants (2022).
[36] Y. Shinbo, Y. Nakamura, M. Altaf-Ul-Amin, H. Asahi, K. Kurokawa, M. Arita, K. Saito, D. Ohta, D. Shibata, S. Kanaya, KNApSAcK: a comprehensive species-metabolite relationship database, in: K. Saito, R.A. Dixon, L. Willmitzer (Eds.), Plant Metabolomics, Springer Berlin Heidelberg, Berlin, Heidelberg, 2006, pp. 165–181, https://doi.org/10.1007/3-540-29782-0_13.
[37] S. Schmidt, M. Zietz, M. Schreiner, S. Rohn, L.W. Kroh, A. Krumbein, Identification of complex, naturally occurring flavonoid glycosides in kale (Brassica oleracea var. sabellica) by high-performance liquid chromatography diode-array detection/electrospray ionization multi-stage mass spectrometry, Rapid Commun. Mass Spectr. 24 (14) (2010) 2009–2022, https://doi.org/10.1002/rcm.4605.
[38] S.E. Bianchi, H.F. Teixeira, S. Kaiser, G.G. Ortega, P.H. Schneider, V.L. Bassani, A bioanalytical HPLC method for coumestrol quantification in skin permeation tests followed by UPLC-QTOF/HDMS stability-indicating method for identification of degradation products, J. Chromatogr. B 1020 (2016) 43–52, https://doi.org/10.1016/j.jchromb.2016.03.012.
[39] M. Li, D. Si, Z. Fu, M. Sang, Z. Zhang, E. Liu, W. Yang, X. Gao, L. Han, Enhanced identification of the in vivo metabolites of Ecliptae Herba in rat plasma by integrating untargeted data-dependent MS2 and predictive multiple reaction monitoring-information dependent acquisition-enhanced product ion scan, J. Chromatogr. B 1109 (2019) 99–111, https://doi.org/10.1016/j.jchromb.2019.02.001.
[40] D. De Beer, A.E. Schulze, E. Joubert, A. De Villiers, C.J. Malherbe, M.A. Stander, Food ingredient extracts of cyclopia subternata (Honeybush): variation in phenolic composition and antioxidant capacity, Molecules. (2012) 14602–14624.
[41] H. Li, H. Wang, P. Dong, H. Li, S. Wang, J. Zhang, Comparative characterization of the metabolites of phloretin and phlorizin in rats using UHPLC-Q-Exactive Orbitrap mass spectrometer, Arab. J. Chem. 17 (3) (2024) 105597, https://doi.org/10.1016/j.arabjc.2023.105597.
[42] A.S. Shalaby, H.H. Eid, R.A. El-Shiekh, O.G. Mohamed, A. Tripathi, A.A. Al-Karmalawy, A.A. Sleem, F.A. Morsy, K.M. Ibrahim, S.H. Tadros, F.S. Youssef, Taming food-drug interaction risk: potential inhibitory effects of citrus juices on cytochrome liver enzymes can safeguard the liver from overdose paracetamol-induced hepatotoxicity, ACS. Omega 8 (29) (2023) 26444–26457, https://doi.org/10.1021/acsomega.3c03100.
[43] K. Morreel, Y. Saeys, O. Dima, F. Lu, Y. Van de Peer, R. Vanholme, J. Ralph, B. Vanholme, W. Boerjan, Systematic structural characterization of metabolites in

Arabidopsis via candidate substrate-product pair networks, Plant Cell 26 (3) (2014) 929–945, https://doi.org/10.1105/tpc.113.122242.
[44] A.M.K. Thamm, Y. Qu, V. De Luca, Discovery and metabolic engineering of iridoid/secoiridoid and monoterpenoid indole alkaloid biosynthesis, Phytochem. Rev. 15 (3) (2016) 339–361, https://doi.org/10.1007/s11101-016-9468-y.
[45] H. Wang, H.-Y. Dong, Y.-F. Liu, J.-L. Liang, H.-S. Liu, Q.-S. Zhao, P.-H. Wei, Iridoid glycosides and flavonoids isolated from the twigs and leaves of callicarpa nudiflora and their anti-inflammatory activities, Chem. Biodivers. 19 (12) (2022) e202200993, https://doi.org/10.1002/cbdv.202200993.
[46] A. van Zadelhoff, J.-P. Vincken, W.J.C. de Bruijn, Facile amidation of non-protected hydroxycinnamic acids for the synthesis of natural phenol amides, Molecules. (2022).
[47] J.B. Park, Isolation and characterization of N-feruloyltyramine as the P-selectin expression suppressor from Garlic (Allium sativum), J. Agric. Food Chem. 57 (19) (2009) 8868–8872, https://doi.org/10.1021/jf9018382.
[48] T.-P. Doan, M. Zhang, J.-P. An, J.-E. Ponce-Zea, V.-H. Mai, B. Ryu, E.-J. Park, W.-K. Oh, Metabolite profiling of allium hookeri leaves using UHPLC-qTOF-MS/MS and the senomorphic activity of phenolamides, Nutrients. (2023).
[49] H. Lohani, A. Kumar, V. Bidarakundi, L. Agrawal, S.Z. Haider, N.K. Chauhan, Identification of fatty acids, amides and cinnamic acid derivatives in supercritical-CO2 extracts of cinnamomum tamala leaves using UPLC-Q-TOF-MSE combined with chemometrics, Molecules. (2024).
[50] N. Arslan Burnaz, M. Küçük, Z. Akar, An on-line HPLC system for detection of antioxidant compounds in some plant extracts by comparing three different methods, J. Chromatogr. B 1052 (2017) 66–72, https://doi.org/10.1016/j.jchromb.2017.03.003.
[51] X. Dai, Q. Huang, B. Zhou, Z. Gong, Z. Liu, S. Shi, Preparative isolation and purification of seven main antioxidants from Eucommia ulmoides Oliv. (Du-zhong) Leaves using HSCCC guided by DPPH-HPLC experiment, Food Chem. 139 (1) (2013) 563–570, https://doi.org/10.1016/j.foodchem.2013.02.006.
[52] X. Hu, H. Zhao, S. Shi, H. Li, X. Zhou, F. Jiao, X. Jiang, D. Peng, X. Chen, Sensitive characterization of polyphenolic antioxidants in Polygonatum odoratum by selective solid phase extraction and high performance liquid chromatography–diode array detector–quadrupole time-of-flight tandem mass spectrometry, J. Pharm. Biomed. Anal. 112 (2015) 15–22, https://doi.org/10.1016/j.jpba.2015.04.018.
[53] D. Tang, H.-J. Li, J. Chen, C.-W. Guo, P. Li, Rapid and simple method for screening of natural antioxidants from Chinese herb Flos Lonicerae Japonicae by DPPH-HPLC-DAD-TOF/MS, J. Sep. Sci. 31 (20) (2008) 3519–3526, https://doi.org/10.1002/jssc.200800173.
[54] D.-L. Li, Y.-L. Zhao, X.-L. Sun, B.-R. Hu, M.-L. Ma, Rapid screening of natural free radical scavengers in two Polygonum herbs by fast HPLC-DAD-ESI-MSn with precolumn incubation method, Anal. Methods 6 (7) (2014) 2299–2305, https://doi.org/10.1039/C3AY41897A.
[55] M. Mnatsakanyan, T.A. Goodie, X.A. Conlan, P.S. Francis, G.P. McDermott, N. W. Barnett, D. Shock, F. Gritti, G. Guiochon, R.A. Shalliker, High performance liquid chromatography with two simultaneous on-line antioxidant assays: evaluation and comparison of espresso coffees, Talanta 81 (3) (2010) 837–842, https://doi.org/10.1016/j.talanta.2010.01.024.
[56] Z.-Q. Ou, D.M. Schmierer, T. Rades, L. Larsen, A. McDowell, Application of an online post-column derivatization HPLC-DPPH assay to detect compounds responsible for antioxidant activity in Sonchus oleraceus L. leaf extracts, J. Pharm. Pharmacol. 65 (2) (2013) 271–279, https://doi.org/10.1111/j.2042-7158.2012.01591.x.
[57] L.G. Korkina, Phenylpropanoids as naturally occurring antioxidants: from plant defense to human health, Cell Mol. Biol. 53 (1) (2007) 15–25.
[58] A.Khatkar Neelam, K.K. Sharma, Phenylpropanoids and its derivatives: biological activities and its role in food, pharmaceutical and cosmetic industries, Crit. Rev. Food Sci. Nutr. 60 (16) (2020) 2655–2675, https://doi.org/10.1080/10408398.2019.1653822.
[59] J.A.B. Peixoto, G. Álvarez-Rivera, A.S.G. Costa, S. Machado, A. Cifuentes, E. Ibáñez, M.B.P.P. Oliveira, R.C. Alves, Contribution of phenolics and free amino acids on the antioxidant profile of commercial lemon Verbena infusions, Antioxidants (2023).
[60] S. Pollastri, I. Baccelli, F. Loreto, Isoprene: an antioxidant itself or a molecule with multiple regulatory functions in plants? Antioxidants. (Basel) 10 (5) (2021) https://doi.org/10.3390/antiox10050684.
[61] J. Flieger, M. Flieger, The [DPPH●/DPPH-H]-HPLC-DAD method on tracking the antioxidant activity of pure antioxidants and goutweed (Aegopodium podagraria L.) hydroalcoholic extracts, Molecules. (2020).
[62] M.C. Foti, C. Daquino, I.D. Mackie, G.A. DiLabio, K.U. Ingold, Reaction of phenols with the 2,2-diphenyl-1-picrylhydrazyl radical. Kinetics and DFT calculations applied to determine ArO-H bond dissociation enthalpies and reaction mechanism, J. Org. Chem. 73 (23) (2008) 9270–9282, https://doi.org/10.1021/jo8016555.
[63] A. Mittal, V.K. Vashistha, D.K. Das, Recent advances in the antioxidant activity and mechanisms of chalcone derivatives: a computational review, Free Radic. Res. 56 (5–6) (2022) 378–397, https://doi.org/10.1080/10715762.2022.2120396.
[64] Y. Park, H.-J. Lee, W.Y. Lee, J.-K. Ahn, B.-H. Hwang, Study on the relationship between the structure and antioxidant activities of chalcones, J. Korean Wood Sci. Technol. 34 (2) (2006) 88–94.
[65] M.K. Samota, D.K. Yadav, P. Koli, M. Kaur, M. Kaur, H. Rani, S.S. Selvan, P. Mahala, K. Tripathi, S. Kumar, Exploring natural chalcones: innovative extraction techniques, bioactivities, and health potential, Sustain. Food Technol. 2 (5) (2024) 1456–1468, https://doi.org/10.1039/D4FB00126E.
[66] R.A. Mendes, B.L.S. e Silva, R. Takeara, R.G. Freitas, A. Brown, G.L.C. de Souza, Probing the antioxidant potential of phloretin and phlorizin through a computational investigation, J. Mol. Model. 24 (4) (2018) 101, https://doi.org/10.1007/s00894-018-3632-9.
[67] T. Yang, Z. Zhang, F. Ning, L. Yuan, X. Yang, L. Luo, New theoretical perspective for easy evaluation of the antioxidant properties of typical flavonoids, Microchem. J. 197 (2024) 109786, https://doi.org/10.1016/j.microc.2023.109786.
[68] Y.Z. Zheng, G. Deng, Q. Liang, D.F. Chen, R. Guo, R.C. Lai, Antioxidant activity of quercetin and its glucosides from Propolis: a theoretical study, Sci. Rep. 7 (1) (2017) 7543, https://doi.org/10.1038/s41598-017-08024-8.
[69] D.N. Olennikov, A.I. Gadimli, J.I. Isaev, N.I. Kashchenko, A.S. Prokopyev, T. N. Kataeva, N.K. Chirikova, C. Vennos, Caucasian Gentiana species: untargeted LC-MS metabolic profiling, antioxidant and digestive enzyme inhibiting activity of six plants, Metabolites. (2019).
[70] M. Tattini, F. Loreto, A. Fini, L. Guidi, C. Brunetti, V. Velikova, A. Gori, F. Ferrini, Isoprenoids and phenylpropanoids are part of the antioxidant defense orchestrated daily by drought-stressed Platanus × acerifolia plants during Mediterranean summers, New. Phytol. 207 (3) (2015) 613–626, https://doi.org/10.1111/nph.13380.
[71] A. López-Munguía, Y. Hernández-Romero, J. Pedraza-Chaverri, A. Miranda-Molina, I. Regla, A. Martínez, E. Castillo, Phenylpropanoid glycoside analogues: enzymatic synthesis, antioxidant activity and theoretical study of their free radical scavenger mechanism, PLoS. One 6 (6) (2011) e20115, https://doi.org/10.1371/journal.pone.0020115.